Journal of Molecular Catalysis A: Chemical 295 (2008) 68–76

Contents lists available at ScienceDirect

Journal of Molecular Catalysis A: Chemical

journal homepage: www.elsevier.com/locate/molcata

Fischer–Tropsch synthesis: The role of pore size for Co/SBA-15 catalysts

Haifeng Xiong[a], Yuhua Zhang[a], Kongyong Liew[b], Jinlin Li[a,b,*]

[a] School of Chemistry and Chemical Engineering, Suzhou University, Suzhou, China
[b] Key Laboratory of Catalysis and Materials Science of the State Ethnic Affairs Commission & Ministry of Education, South-central University for Nationalities, Wuhan, China

ARTICLE INFO

Article history:
Received 21 May 2008
Received in revised form 7 August 2008
Accepted 30 August 2008
Available online 5 September 2008

Keywords:
Fischer–Tropsch synthesis
Pore size
Cobalt catalysts
SBA-15

ABSTRACT

Co/SBA-15 (30 wt.%) catalysts with different pore sizes were prepared from the same materials by incipient wetness impregnation and characterized by diffuse reflectance infrared Fourier transform spectroscopy, N_2 adsorption–desorption, X-ray diffractometry, temperature-programmed reduction and H_2 desorption, oxygen titration as well as transmission electron microscopy. The reduction of the catalysts took place in two stages with Co_3O_4 reduction to CoO and then to Co^0. The first stage reduction was facile regardless of the catalyst pore size while the second stage reduction was much easier on the catalysts with larger pore. After the reduction, cobalt particles were found to be distributed on both the exterior and interior surfaces of the support. Compared to the catalyst with smaller pores, larger pore catalysts have more adsorption sites for CO of both the linear and bridge types. The catalysts with larger pore led to larger cobalt cluster size, lower dispersion and higher reducibility. The larger pores gave rise to more adsorbed CO of the bridge-type on FTS. CO conversion increased and then decreased with the pore size in the range studied. The catalysts with larger cobalt cluster size showed higher C_{5+} selectivity for the FTS.

1. Introduction

The costs of crude oil have been increasing to well above US$ 100 per barrel now. Fischer–Tropsch synthesis (FTS) technology which is a chemical process for the production of liquid fuel has thus become more attractive [1]. Cobalt FTS catalysts are preferred because these catalysts have low activity for the water–gas shift reaction, deactivate less rapidly and yield a higher fraction of linear paraffin than iron catalyst [2]. High cobalt loading is necessary to achieve high activity and to stabilize the catalyst against deactivation due to reoxidation [3,4]. As for the current commercial cobalt-based catalyst of choice for slurry bubble column reactor, the cobalt loading is very high at 33 g per 100 g support [5]. Therefore, high surface area support is necessary to disperse such high cobalt content.

SBA-15 is a silica-based mesoporous material with uniform hexagonal channels ranging from 3 to 30 nm with narrow pore size distribution [6]. It is one of the most attractive catalyst supports with high hydrothermal stability and large surface area of 600–1000 m^2/g, allowing for the dispersion of a large number of catalytically active species. Besides, the reducibility is favored for the SiO_2 supported Co catalyst because the strength of interaction between the cobalt and support is lower than the other commonly used supports [7,8]. Thus, SBA-15 possesses the characteristics of a potential support for the preparation of a commercial FTS cobalt catalyst with high activity.

According to previous investigation [2], FTS turnover rates are independent of the Co dispersion and support identity over the accessible dispersion range (0.01–0.12) at typical FTS conditions. High productivity for supported cobalt-based FTS catalysts requires small cobalt crystallites at high cobalt surface densities. It is well known that the smaller the cobalt particle size, the stronger the interaction between cobalt and support. Strong interaction between the cobalt and support decreases both the catalyst reducibility and activity for FTS. To prepare highly active cobalt based catalyst, it is necessary to balance precisely between dispersion and reducibility.

It has been reported by Anderson et al. that the FTS activity and selectivity of cobalt based catalyst could be affected by their pore sizes [9]. The observed increase in methane selectivity with decreasing average pore size was attributed to mass transport phenomenon. Later, Lapszewicz et al. [10] showed that the variation of product distribution as a function of catalyst pore diameter was a result of the change of adsorption patterns of hydrogen and carbon monoxide. Recently, Panpranot et al. [11] reported a significant increase in CO hydrogenation when silica MCM-41 was used as the support. However, Khodakov et al. [12] studied pore size effects in FTS over cobalt-supported mesoporous silicas (SBA-15 and MCM-41) and concluded that FTS rates were much higher

* Corresponding author at: School of Chemistry and Chemical Engineering, Suzhou University, Suzhou, China. Tel.: +86 27 67843016; fax: +86 27 67842752.
E-mail address: jinlinli@yahoo.cn (J. Li).

1381-1169/$ – see front matter © 2008 Elsevier B.V. All rights reserved.
doi:10.1016/j.molcata.2008.08.017

on cobalt catalysts with pore diameter exceeding 3 nm than on narrow pore catalysts. They showed that the reducibility and the size of supported cobalt species depended strongly on the pore size, and increased with increasing pore diameter. In this case, the cobalt loading was low (5 wt.%) and silicas from different origin were employed. It has been suggested that the support variations may have caused the differences in the results [13]. These works suffered from the deficiencies of either the cobalt content was much lower than the commercial catalysts [11,12] or different support materials with unknown impurities were used [10–12].

In the present study, high cobalt loading catalysts (30 wt.%) with supports of different pore sizes were thus prepared by the same method ensuring that no other interference was involved. A systematic study of the effect of pore size on the activity and selectivity of FTS over SBA-15 supported cobalt catalysts was then carried out using this series of catalysts.

2. Experimental

2.1. Sample preparation

SBA-15 molecular sieves with different pore sizes were prepared using Pluronic P123 ($EO_{20}PO_{70}EO_{20}$, M_{AV} = 5800, BASF) and tetraethyl orthosilicate (TEOS, AR) under acidic conditions following the method reported previously [6]. The narrow pore size silica, labeled as SBA-(1), was synthesized without any hydrothermal treatment. The detailed synthesis route was as follows: P123 (10 g) and 2 M HCl (350 mL) were mixed at 35 °C to obtain a clear solution. Subsequently, TEOS (21 g) was gradually added to the solution and stirred for 48 h. The materials were obtained by filtration and washing with deionized water. Similar to the preparation of SBA-(1), SBA-(2) and SBA-(3) were obtained after a hydrothermal treatment for 24 h, at 100 and 130 °C, respectively. The fourth silica, labeled as SBA-(4), was obtained with the addition of 1,3,5-tri-methylbenzene (TMB, 3 mL) prior to TEOS. The reaction condition was the same as that of SBA-(3). Finally, the obtained materials were transferred to a muffle furnace and calcined at 500 °C for 5 h.

30 wt.% Co/SBA-15 catalysts with different pore sizes were prepared by incipient wetness impregnation of the respective SBA-15 with the desired amount of aqueous cobalt nitrate. The precursor was dried at 120 °C for 12 h, followed by calcination at 400 °C for 5 h. These samples were labeled as 30% Co/SBA-(n) with n standing for 1, 2, 3 or 4.

2.2. Catalyst characterization

A Brukers D8 powder X-ray diffractometer with monochromatic Cu Kα radiation and Ni filter equipped with a VANTEC-1 detector was used for the XRD measurement. A reactor cell (Anton Paar) mounted on a goniometer was used for in situ measurement under different gas atmosphere. Prior to the XRD measurement, the calcined catalysts were flushed with high purity argon at 150 °C for 1 h, to drive away the water and other impurities, and then, cooled down to 30 °C. The diffractograms were recorded from 20° to 80° with 0.016° steps. Crystallite phases were determined by comparing the diffraction patterns with those in the standard powder XRD files (JCPDS) published by the International Center for Diffraction Data. After catalyst was reduction in 450 °C for 8 h, Co particle size was calculated using the Scherrer equation ($d = (0.89\lambda/B\cos\theta)(180°/\pi)$) from the most intense Co peak ($2\theta = 44.2°$). Where d is the cobalt particle diameter, λ is the X-ray wavelength (1.54056 Å), and B is the full width half maximum (FWHM) of Co diffraction peak.

N_2 adsorption–desorption experiment was conducted at −193 °C using a Quantachrome Autosorb-1. Prior to the experiment, the sample was outgassed at 200 °C for 6 h. The surface area was obtained using BET model for adsorption data in a relative pressure ranged from 0.05 to 0.30. The total pore volumes were calculated from the amount of N_2 vapor adsorbed at a relative pressure of 0.99. The pore size distribution were evaluated from the desorption branches of the isotherms using the Barrett–Joyner–Halenda (BJH) method.

TPR experiment was carried out with a Zeton Altamira AMI-200 unit. The catalyst (ca. 0.06 g) was placed in a quartz tubular reactor, fitted with a thermocouple for continuous temperature measurement. The reactor was heated with a furnace designed and built to stabilize the temperature gradient and minimize the temperature error. Prior to the hydrogen temperature-programmed reduction measurement, the calcined catalysts were flushed with high purity argon at 150 °C for 1 h, to drive away the water or impurities, and then, cooled down to 50 °C. Then 10% H_2/Ar was switched on and the temperature was raised at a rate of 10 °C/min from 50 to 800 °C (hold 30 min). The gas flow rate through the reactor was controlled by three Brooks mass flow controllers and was always 30 cm^3 min^{-1}. The H_2 consumption (TCD signal) was recorded automatically by a PC.

Hydrogen temperature-programmed desorption was also carried out in a U-tube quartz reactor with the Zeton Altamira AMI-200 unit. The sample weight was about 0.100 g. The catalyst was reduced at 450 °C for 12 h using a flow of high purity hydrogen and then cooled to 100 °C under hydrogen stream. The sample was held at 100 °C for 1 h under flowing argon to remove weakly bound physisorbed species prior to increasing the temperature slowly to 450 °C. At that temperature, the catalyst was held under flowing argon to desorb the remaining chemisorbed hydrogen and the TCD began to record the signal till the signal returned to the baseline. The TPD spectrum was integrated and the amount of desorbed hydrogen was determined by comparing to the mean areas of calibrated hydrogen pulses. Prior to the experiments, the sample loop was calibrated with pulses of nitrogen in helium flow, comparing with the signal produced from a gas tight syringe injection (100 μL) of nitrogen under helium flow. O_2 titration was also performed with the Zeton Altamira AMI-200 unit. The extent of cobalt reduction was determined by O_2 titration of reduced samples at 450 °C. After reduction under the conditions (as described above for H_2-TPD), the catalysts were kept in flowing Ar at 450 °C and the sample was reoxidized by injecting pulses of high purity oxygen in argon. The extent of reduction was calculated by assuming metal Co was converted to CoO [12,13]. All flow rates were set to 30 cm^3 min^{-1}. The uncorrected dispersions and cluster size are based on the assumption of complete reduction, and the corrected dispersions and cluster size are reported by percentage reduction. The formula for the calculation has been shown in previous studies [14,15].

The TEM images were obtained using an FEI Tecnai G20 instrument. An ex situ reduction step was used to treat the catalysts. The pre-treatment was carried out in an AMI-200 unit. Firstly, the sample was reduced at 450 °C for 10 h. Subsequently, the temperature was decreased to 30 °C and then, 1% O_2/He (30 cm^3/min) was introduced into this system and to passivate the sample for 6 h. After these steps, the passivated catalysts were taken out and suspended in ethanol with ultrasonication. A copper microscope grid covered with perforated carbon was dipped into the solution.

DRIFTS spectra were recorded with a Nicolet NEXUS 670 FTIR spectrometer supplied with a MCT detector and a diffuse reflectance attachment using a spectral resolution of 4 cm^{-1}. The high purity carbon monoxide (>99.999%) was used as the probe gas. Helium and hydrogen (>99.999%) were used as the flushing gas and the reducing gas, respectively. In order to compare the behavior of the intensities of IR bands among the studied catalysts, the amount of samples used should be the same for all the

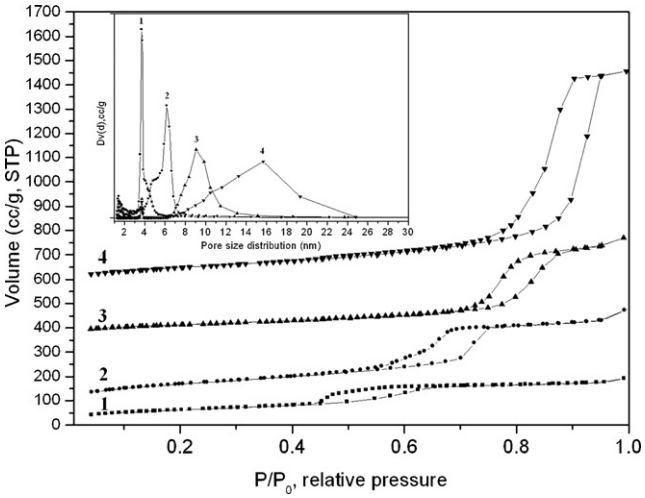

Fig. 1. N_2 adsorption–desorption isotherms and pore size distribution (inset) of 30% Co/SBA-15 catalysts with different pore sizes. (1) 30% Co/SBA-1, (2) 30% Co/SBA-2, (3) 30% Co/SBA-3, (4) 30% Co/SBA-4.

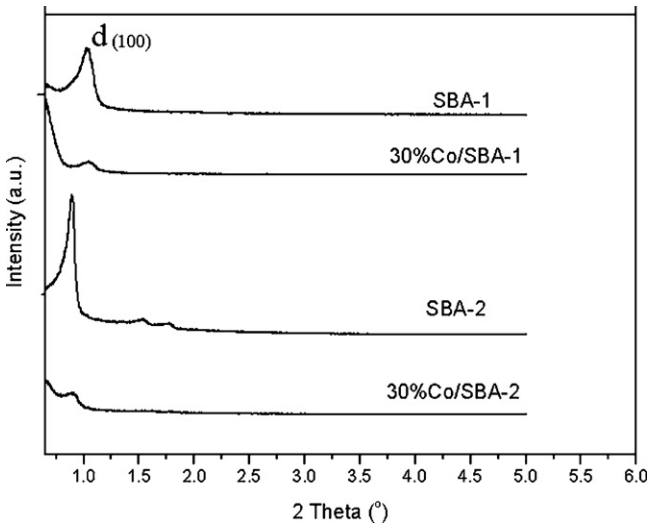

Fig. 2. Typical small angle X-ray diffraction of different materials.

experiments. The catalyst (ca. 5 mg) was placed in an infrared cell with ZnSe windows. The catalyst was reduced in situ for 12 h under atmospheric pressure with a stream of hydrogen at 450 °C at a flow of 20 cm^3 min^{-1}. For the spectra of CO chemisorbed on catalyst, the system was cooled down to 30 °C and the background spectrum was collected. After introduction of carbon monoxide (30 cm^3 min^{-1}) for 2 h, the catalyst was purged with He (flow rate = 20 cm^3 min^{-1}) for 30 min to remove gaseous carbon monoxide before the IR spectra were recorded. For the spectra of catalysts under FTS conditions, the system was cooled down to the desired temperatures (200 and 220 °C) and the respective background spectrum was collected. Subsequently, CO/H_2 mixture ($CO:H_2$ = 1:2, 30 cm^3 min^{-1}) was introduced and the spectra were collected in the presence of He for 30 min after 2 h exposure.

2.3. Catalyst evaluation

Fischer–Tropsch synthesis was performed in a tubular fixed bed reactor (i.d. = 12 mm). The catalyst (0.5 g, 2–10 μm) was mixed with 5 g carborundum and reduced in high purity H_2 (6 SL h^{-1} g^{-1}) at atmosphere pressure. The reactor temperature was increased from ambient to 100 °C (hold 60 min), then, increased to 450 °C in 2 h and held at that temperature for 10 h. Subsequently, the reactor was cooled down to 150 °C. Then, the syngas (CO/H_2 = 1:2, 8 SL h^{-1} g^{-1}) was switched on and the pressure was increased to 2.0 MPa. The reactor temperature was raised to 210 °C at 1 °C/min and the reaction was carried out at 210 °C. The thermocouple used in the experiment showed that temperature gradients along the fixed bed were less than ±1.5 °C. The products were collected in a hot trap (130 °C) and a cold trap (−2 °C) in sequence. The outlet gases were analyzed online by an Agilent 3000 GC and the oil collected at −2 °C was analyzed by an Agilent 6890 GC. Analysis of solid wax collected at 130 °C was performed by an Agilent 4890 GC.

3. Results and discussion

3.1. Sample characterization

3.1.1. Sample porosity

N_2 adsorption–desorption isotherms and pore size distribution of the 30% Co/SBA-15 catalysts are displayed in Fig. 1. All isotherms are type which exhibit the condensation and evaporation steps characteristic of periodic mesoporous materials. The BET surface areas are in the expected range (Table 1). Compared to the respective supports, the cobalt loaded catalysts showed significantly lower BET surface area, pore volume and slightly smaller average pore size. This suggested that part of the cobalt species have entered into the pore of the support [16].

3.1.2. X-ray diffraction

In the small angle region of XRD (Fig. 2), the as-synthesized SBA-15 exhibits intense diffraction peaks, characteristic of the hexagonal (*p6mm*) structure. After introduction of the cobalt species (30 wt.% Co), the intensity of these diffraction peaks decreased. This suggested that the mesoporous structure of the catalyst may be partially destroyed. It is different from the results of Khodakov et al. [17]. In their reports, although aqueous impregnation had an impact on the long range ordering and mesoporous structure of the support, the impact of aqueous impregnation on SBA-15 was very small.

Table 1
N_2 adsorption–desorption and cobalt particle size data of samples

Samples	Surface area (m^2/g)	Total pore volume (cm^2/g)	Pore diameter (nm)	Thickness of the pore wall[a] (nm)	Co particle size (nm)
SBA-1	826.72	0.74	3.68	6.4	–
SBA-2	896.61	1.37	6.46	3.1	–
SBA-3	498.55	1.23	9.32	3.5	–
SBA-4	530.71	2.51	15.78	4.0	–
30Co/SBA-1	369.60	0.37	3.71	6.5	11.72
30Co/SBA-2	473.60	0.69	6.17	3.6	12.25
30Co/SBA-3	323.2	0.65	9.0	3.9	14.68
30Co/SBA-4	350.35	1.41	15.5	4.2	16.25

[a] The thickness of pore wall were calculated as: α_0-pore size ($\alpha_0 = 2 \times d(100)/\sqrt{3}$).

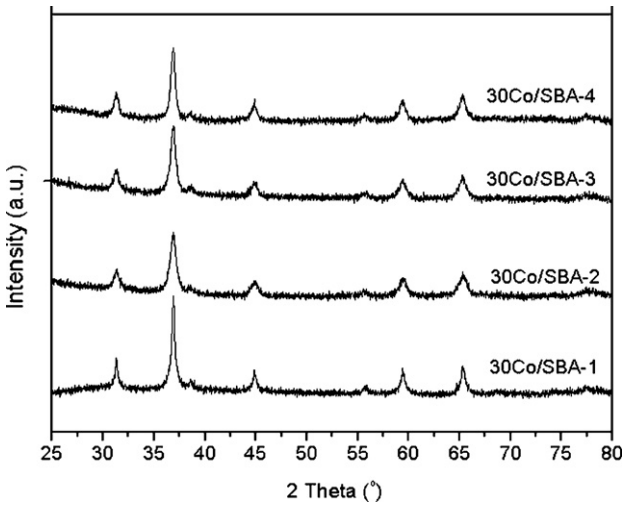

Fig. 3. X-ray diffraction of different 30% Co/SBA-15 catalysts.

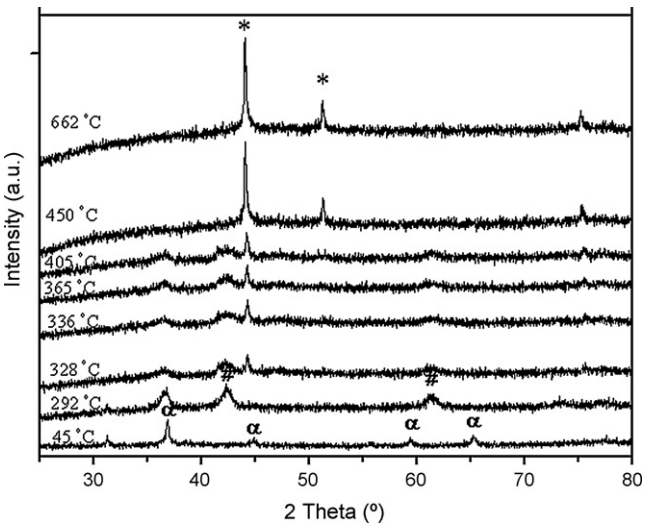

Fig. 4. In situ X-ray diffraction of 30% Co/SBA-1 catalyst in 10% H_2/Ar (30 cm^3 min^{-1}); α: Co_3O_4, #: CoO, *: Co^0 (cubic).

Fig. 3 displays the XRD patterns of the prepared 30% Co/SBA-15 catalysts. Similar diffraction peak positions are shown for all catalysts, indicating that similar phases were dispersed on the surface. The peaks at 31.4°, 36.9°, 44.8°, 59.4°, 65.2° correspond to the different crystal planes of Co_3O_4 phase. No other crystalline phase was detected on the prepared cobalt catalysts.

The in situ XRD patterns of the 30% Co/SBA-15 samples with different pore sizes under 10% H_2/Ar were measured. Typically, as shown in Fig. 4, reduction of 30% Co/SBA-1 in 10% H_2/Ar at atmospheric pressure took place in two stages, with Co_3O_4 reduction

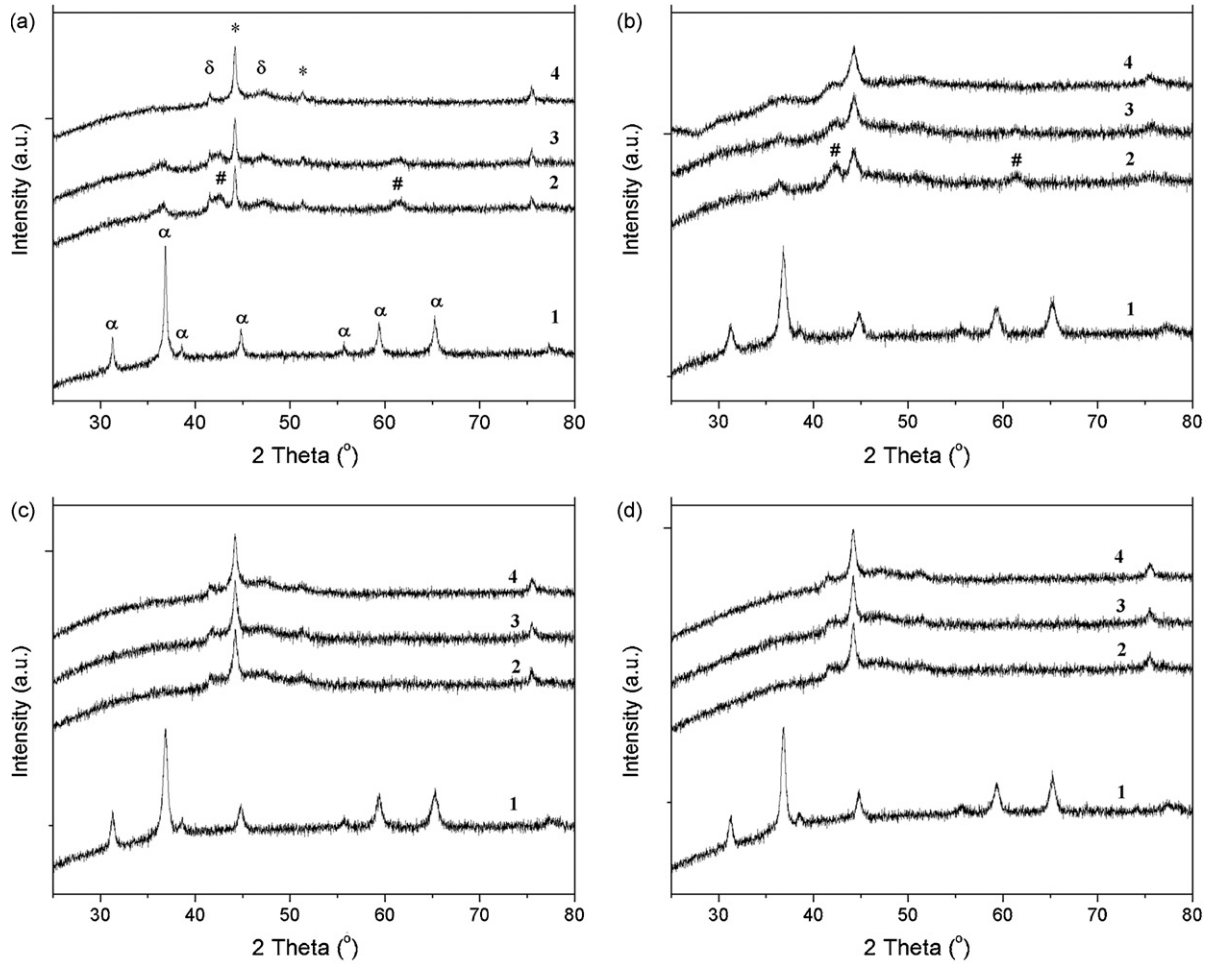

Fig. 5. In situ X-ray diffraction of catalysts in pure H_2 (30 mL/min). (a) 30% Co/SBA-1, (b) 30% Co/SBA-2, (c) 30% Co/SBA-3, (d) 30% Co/SBA-4. (1) Room temperature, (2) reaching 450 °C, (3) 450 °C for 2 h, (4) 450 °C for 10 h; α: Co_3O_4, #: CoO, *: Co^0 (cubic), δ: Co^0 (hexagonal).

to CoO and CoO reduction to Co^0. The first stage was completed at around 292 °C. The second stage occurred at <328 °C and was completed at <450 °C. The XRD pattern of 30% Co/SBA-1 measured in situ during reduction under pure H_2 is shown in Fig. 5a. Two reduction steps were also observed on increasing the reduction temperature. However, compared to the reduction under 10% H_2/Ar, reduction at 450 °C in high purity H_2 apparently led to the formations of both the cubic phase and hexagonal phase of Co^0, but only the cubic phase was observed in 10% H_2/Ar at 450 °C. Cobalt has a close-packed hexagonal structure, but transforms to a face-centered cubic structure at ~417 °C [18]. This suggests that the reduction in H_2 could enhance the formation of hexagonal phase more than reduction in 10% H_2/Ar. It should be mentioned that 30% Co/SBA-1 catalyst was completely reduced in the mixture 10% H_2/Ar (Fig. 4) while with pure H_2 and after 2 h some CoO is still present (Fig. 5a-3). It is an unexpected phenomenon. A possible explanation is that Co_3O_4 was firstly reduced to CoO and the CoO particle size produced in pure H_2 is larger, but CoO particle size produced in 10% H_2/Ar is smaller. The larger CoO particles can be detected and the smaller CoO particles are missed by XRD because CoO particles are probably too fine (<40 Å) for XRD [19]. It has been reported that the reduction carried out using pure H_2 and 5% H_2/He gave different cobalt metal particles [20].

The in situ XRD patterns of 30% Co/SBA-15 catalysts reduced at 450 °C under H_2 are shown in Fig. 5. For all the catalysts, as can be seen, the reduction with H_2 for 10 h resulted in the complete reduction of the Co_3O_4 to CoO and to metal Co. When the reduction temperature reached 450 °C, Co_3O_4 phase of all the catalysts transformed to CoO, indicating that Co_3O_4 reduction is fast regardless of the catalyst pore size. However, the diffraction peaks of CoO for 30% Co/SBA-1 and 30% Co/SBA-2 still remained even after reduction in H_2 at 450 °C for 2 h while for larger pore size catalysts, these peaks have disappeared completely when the reduction temperature reached 450 °C. This suggests the much easier reduction of CoO phase to Co for the larger pore catalyst, in agreement with earlier works [21–23].

3.1.3. Temperature-programmed reduction

The TPR spectra of 30% Co/SBA-15 catalysts with different pore sizes are shown in Fig. 6. The recorded curves showed three main reduction regions. Correlated with the above in situ XRD data under 10% H_2/Ar, the first reduction peak at 220–320 °C can be attributed to the first reduction step of Co_3O_4 ($Co_3O_4 \rightarrow CoO$). The second reduction region at 320–550 °C is attributed to the reduction of intermediate CoO phase ($CoO \rightarrow Co^0$). According to the literature [7], for small pore catalyst, the high temperature reduction peak at 670 °C is attributed to the reduction of interaction compound (Co_2SiO_4), although no Co_2SiO_4 phase is observed in XRD measurement in the present study. It can be seen that the TPR spectra of both 30% Co/SBA-3 and 30% Co/SBA-4 have not exhibited the reduction of interaction compound Co_2SiO_4. The pore size markedly affected the reduction processes of 30% Co/SBA-15 catalysts. Firstly, with the increase of catalyst pore size, the reduction peak at high temperature disappeared and the intensity of reduction peak at 200–450 °C increased. Secondly, for 30% Co/SBA-1 catalyst, the positions of the reduction peaks shifted to higher temperature compared to the catalysts with larger pore sizes. Both of these indicate that the smaller pore size cobalt catalyst was more difficultly reduced. It is believed that the first reduction step of Co_3O_4 to CoO is fast (giving a sharp low-temperature peak) while the CoO reduction step is slow, resulting a broad profile. This can be seen in Fig. 6. The broadening is considered to depend on the interaction between CoO and the support and the TPR profile depends on cluster size. The smaller CoO clusters are considered to interact more strongly with the support than larger ones [23]. In the present study, Co particle size on 30% Co/SBA-15 catalysts increased with increasing catalyst pore sizes (Table 1), leading to the disappearance of interaction compound (Co_2SiO_4) and the narrowing of the second reduction step ($CoO \rightarrow Co^0$). It should be mentioned that the second reduction region of several catalysts was comprised of more than one peak, which is explained by the effect of different-sized particles giving rise to varying degrees of interaction between the cobalt and support [13].

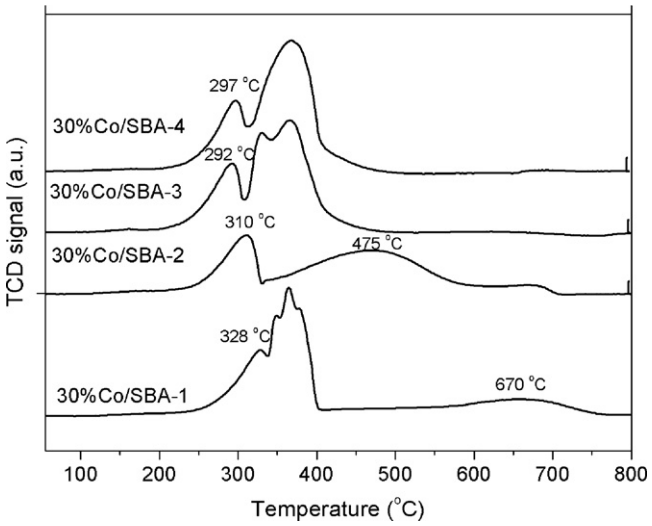

Fig. 6. TPR spectra of 30% Co/SBA-15 catalysts with different pore sizes.

3.1.4. Transmission electron microscopy

The representative TEM images of 30% Co/SBA-15 catalysts after reduction and passivation is shown in Fig. 7, cobalt was distributed on the exterior surface (Fig. 7a and d) and interior surface (Fig. 7b) of the support and the particle size distribution is wide. For such a high cobalt loading, cobalt exists as clusters (Fig. 7c) and some clusters are agglomerated to form islands (Fig. 7a) consisting of many small particles. It is difficult to obtain the cobalt particle size from the TEM micrograms because the contrast between the metal and support is not sufficiently clear [24–26].

Table 2
H_2-TPD data and O_2 titration data of prepared 30% Co/SBA-15 catalysts with different pore sizes

Sample	H_2 desorbed (μmol g^{-1})	d_{uncorr} [a] (%)	D_{uncorr} [b] (nm)	O_2 uptaked (μmol g^{-1})	Extent of reduction (%)	d_{corr} [c] (%)	D_{corr} [d] (nm)
30% Co/SBA-1	64.7	2.54	40.6	1705.8	50.01	5.08	20.30
30% Co/SBA-2	49.5	1.95	53	1694.9	49.70	3.92	26.34
30% Co/SBA-3	47.3	1.86	55.5	1863.4	54.63	3.41	30.32
30% Co/SBA-4	23.8	0.94	110.2	1960.6	57.49	1.64	63.35

[a] The uncorrected catalyst dispersion.
[b] The uncorrected metal cluster diameter.
[c] The corrected catalyst dispersion.
[d] The corrected metal cluster diameter.

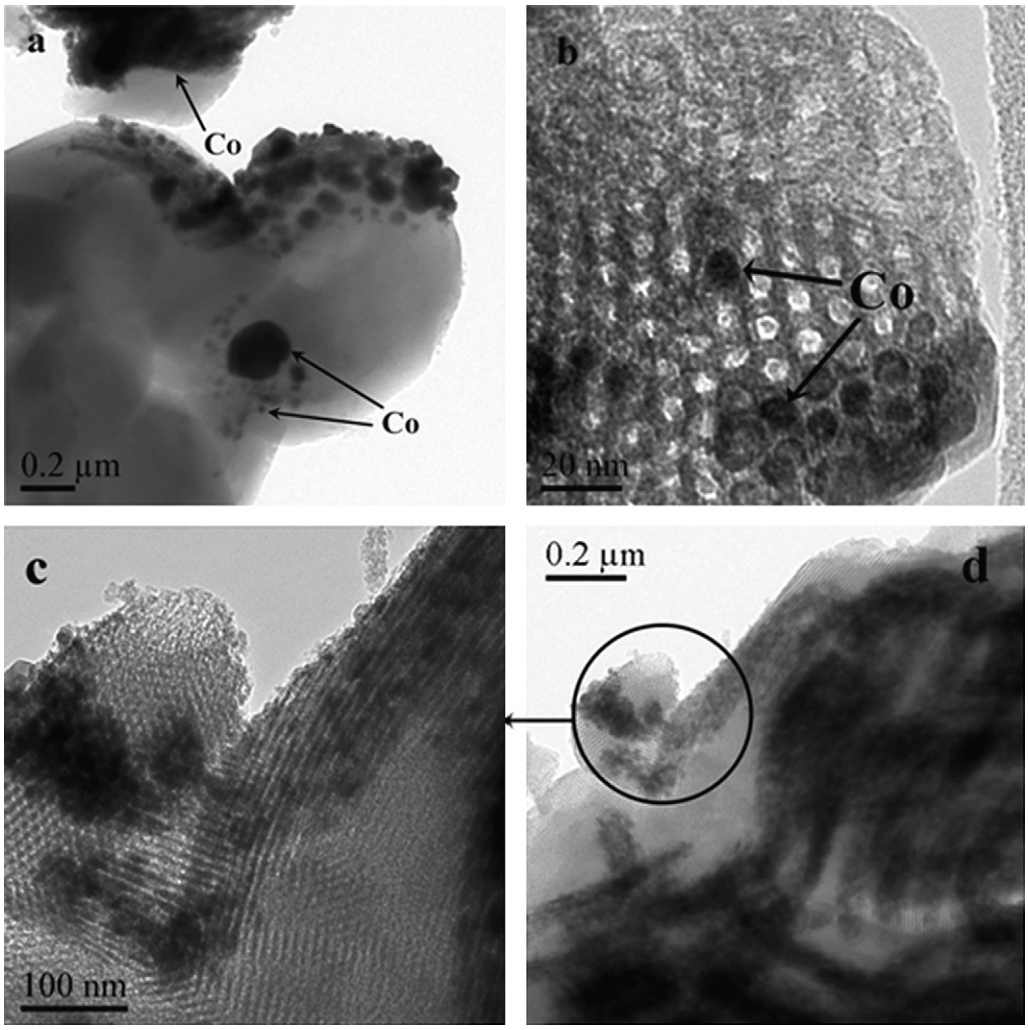

Fig. 7. TEM images of passivated 30% Co/SBA-15 catalysts in the flow of 1% O_2/He after reduction under H_2 for 10 h. (a) Perpendicular to the *c* axis for 30% Co/SBA-1, (b) parallel to the *c* axis for 30% Co/SBA-2, (c) higher magnification image for 30% Co/SBA-2, (d) low magnification image for 30% Co/SBA-2.

3.1.5. H_2 chemisorption and oxygen titration

The data for hydrogen chemisorption and O_2 titration are present in Table 2. As can be seen, the catalyst pore size significantly affected the metal cobalt particle size, dispersion and reducibility. The corrected dispersion and cluster size were used to explain the effect of catalyst pore size on dispersion and cluster size. With increasing catalyst pore size, cobalt dispersion decreased from 5.08 to 1.64%, and catalyst reducibility increased from 50.01 to 57.49%. The increase of catalyst reducibility is consistent with the TPR results. The metal cobalt particle size increases significantly with increasing catalyst pore size, which is in agreement with XRD result (Table 1). The effect of pore size on the reducibility and dispersion is in agreement with the result for cobalt supported alumina catalysts [13,27].

3.1.6. Diffuse reflectance infrared Fourier transform spectroscopy (DRIFTS)

The surface properties of Co species on the supported cobalt catalysts after reduction can be obtained by IR spectroscopy with CO as the probe molecule. The spectra of CO chemisorbed on the surface of the 30% Co/SBA-15 catalysts after reduction with H_2 at 450 °C for 12 h are shown in Fig. 8. For 30% Co/SBA-1 catalyst, at room temperature, four bands located at 2061, 2036, 1978 and 1936 cm^{-1} are clearly resolved, in addition to two broad peaks appearing at 2171

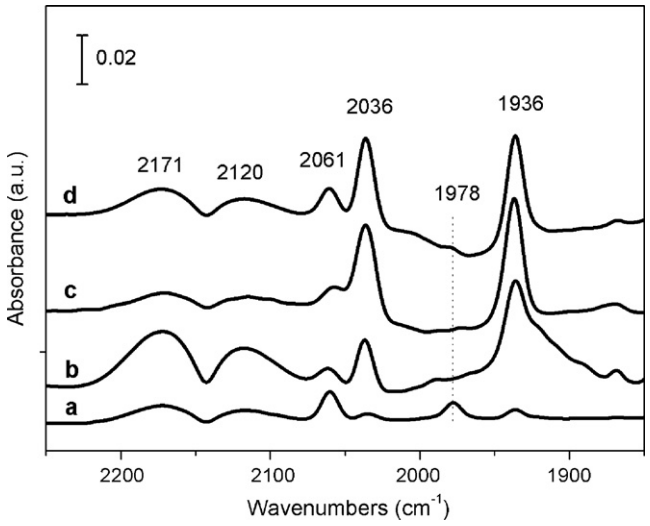

Fig. 8. FTIR spectra collected following adsorption of CO at room temperature on 30% Co/SBA-15 pretreated in H_2 at 450 °C for 12 h and subsequent desorption in He at room temperature for 30 min. (a) 30% Co/SBA-1, (b) 30% Co/SBA-2, (c) 30% Co/SBA-3, (d) 30% Co/SBA-4.

Table 3
Performances of 30% Co/SBA-15 with different pore sizes in a fixed bed reactor

Catalyst	X_{co} (%)	Hydrocarbon selectivity				
		CH_4	C_2	C_3	C_4	C_{5+}
30% CO/SBA-1	19.32	10.76	1.62	6.55	5.69	75.38
30% CO/SBA-2	41.78	7.11	1.55	5.64	5.08	80.62
30% CO/SBA-3	30.88	7.05	0.53	2.38	2.58	87.46
30% CO/SBA-4	24.21	7.36	0.33	2.05	2.78	87.48

Reaction conditions: 2.0 MPa, 210 °C, CO/H = 1:2, GHSV = 8 SL h^{-1} g^{-1}.

Table 4
Assignement of the infrared bands observed in the spectra of CO adsorbed on 30% Co/SBA-15 catalysts

Frequencies	Assignment
2171,2120	Assignment to CO absorbed on trivalent and divalent cations
2061	Assigned to CO species on metallic cobalt with weak electron–donor properties (with partial positive charge $Co^{\delta+}$)
2036	CO absorbed on zerovalent Co^0 sites in a linear geometry
1978	CO absorbed in bridged position
1936	CO absorbed in bridged position, which is slightly different with 1978 cm^{-1}

and 2120 cm^{-1}. As can be seen, the spectral pattern changes significantly with increasing cobalt catalyst pore size. First of all, the intensity of the band at 1978 cm^{-1} decreased. Secondly, the intensity of the band at 1936 cm^{-1} increased greatly when the pore size was increased from 3.68 to 6.46 nm, while no significant change was observed on further increase of pore size. Thirdly, compared to 30% Co/SBA-1 catalyst, the band intensity at 2061 cm^{-1} decreased to some extent with increasing catalyst pore size. Besides, the band intensity at 2036 cm^{-1} increases with increasing pore size. It should be mentioned that all peak positions were not significantly shifted with the increase of catalyst pore size and that the band shapes developed after increasing the desorption temperature were nearly identical (not shown here). With increasing desorption temperature, the intensity of all band decreased by degrees and the wave number of the intensity maximum was temperature independent. This suggests that no new cobalt absorption site appeared with the change of pore size.

Most of these bands have been observed previously as indicated in the literatures for cobalt based catalyst supported on traditional supports [28–32], although the assignments of some of them remain under debate. However, there is a general agreement that the bands between 2100 and 2000 cm^{-1} can be assigned to linearly adsorbed CO and those below 2000 cm^{-1} can be ascribed to bridge-type CO adsorption on Co^0 crystallites. A number of studies have assigned the bands at 2171 and 2120 cm^{-1} to the residual gaseous carbon monoxide in the cell [29,33]. Others have argued that the bands should be assigned to CO absorbed on trivalent and divalent cations [34–37]. Although there is no direct evidence regarding the assignments of the bands in the present study, we believed that it should be assigned to the CO adsorbed on relatively high oxidation state cations (Co^{2+}, Si^{2+}) through donating its electrons in σ-type coordination bond because the high-frequency band of gaseous CO should be located at 2143 cm^{-1} [34]. Kadinov et al. [38] attributed the band at 2061 cm^{-1} to a structure of hydrocarbonyl. Rygh et al. [31,32] assigned the band around 2060 cm^{-1} to overlapping contributions from $Co(CO)_n$, CoHCO, $Co^{\delta+}$-CO, and large islands of CO^0-CO on Co(0 0 0 1). It was reported that the hydrocarbonyl is quite unstable and the formation of hydrocarbonyl is a requisite intermediate step in the overall reaction between coadsorbed hydrogen and CO [39]. We found that the intensity of the band at 2061 cm^{-1} of 30% Co/SBA-1 was strongest among the catalysts, while its activity was the lowest (see Table 3 below). We propose that the band at 2061 cm^{-1} can be assigned to CO species on metallic cobalt with weak electron–donor properties (with partial positive charge $Co^{\delta+}$) [40]. There is general agreement that the band at 2036 cm^{-1} can be assigned to CO adsorbed on zerovalent Co^0 sites in a linear geometry [28–34,37,41]. The peaks at 1978 and 1936 cm^{-1} can be assigned to the bridge-type CO adsorbed on metal cobalt. The band intensity at 1978 cm^{-1} decreased with the increase of catalyst pore size, while the band intensity at 1936 cm^{-1} increased. This suggested that two bands (1978 and 1936 cm^{-1}) were derived from different bridge-type CO species. The assignment of the infrared bands observed in the spectra of CO adsorbed on 30% Co/SBA-15 catalysts was shown in Table 4.

The DRIFTS spectra of 30% Co/SBA-15 with different pore sizes under FTS conditions are shown in Fig. 9. When the spectra were collected at 220 °C, a broad peak located at 1979 cm^{-1} was observed, which can be assigned to bridge-type CO on cobalt metal sites. With the increase of catalyst pore sizes, the intensity of bridge-type CO band increases significantly. In contrast with the CO adsorption experiments at room temperature and the investigations of Morales et al. [29], none of the catalysts at 220 °C exhibited any CO adsorption band in linear geometry in the present study. It

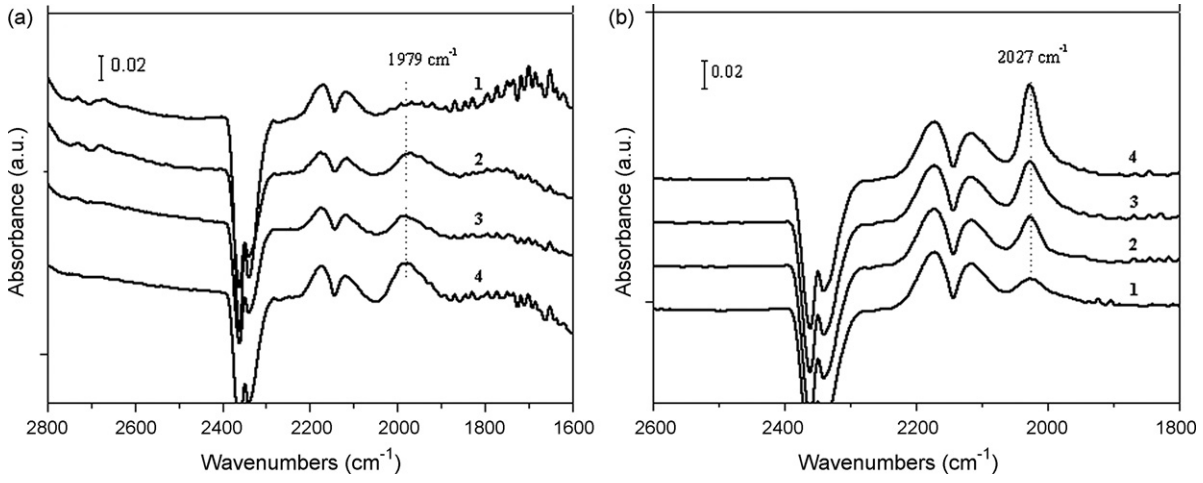

Fig. 9. DRIFTS spectra of 30% Co/SBA-15 with different pore sizes after 2 h exposure to syngas ($CO:H_2$ = 1:2). (a) At 220 °C, (b) at 200 °C. (1) 30% Co/SBA-1, (2) 30% Co/SBA-2, (3) 30% Co/SBA-3, (4) 30% Co/SBA-4.

is of interest to note that a narrow band centered at 2027 cm^{-1} for 30% Co/SBA-15 catalysts was observed when the spectra were collected under FTS condition (200 °C). This band should be assigned to CO linearly adsorbed on cobalt metal sites and no bridge-type CO was found. With the increase of catalyst pore sizes, the intensity of CO band in linear geometry increases significantly. Compared to the results, it is suggested that this band shifted from 2029 cm^{-1} at 200 °C to 1979 cm^{-1} at 220 °C because of the decreasing CO coverage and hence the reduced CO coupling effect. It has been reported that it is possible for the conversion of linear to bridge type CO species before desorption at higher temperature [42,43].

3.2. Fischer–Tropsch synthesis

The data of FTS activity and product selectivity for the catalysts are listed in Table 3. As can be seen, CO conversion is found to increase and then decrease with increasing pore size in the range studied. The selectivity to C_{5+} hydrocarbons increases with the increase in pore size initially and finally remained unchanged.

The pore size can affect the rate of FTS for pore-confined Ru catalyst [44]. However, for the current study, most of the cobalt particles on 30% Co/SBA-15 prepared by impregnation were dispersed on the external surface of the catalyst as islands after reduction, as shown from the TEM images. Iglesia et al. [45,46] showed that FT synthesis rates were proportional to the metal dispersion and were independent of the support. They attributed lower activity of small cobalt particles observed in previous reports to the differences in the extent of reduction as a function of metal dispersion, chemical identity, and surface properties of the support [12]. It is believed that the bridge-type CO was more easily formed on large Co particle and was much more active than linear-type CO because it has a weaker C—O bond and thus can be more easily dissociated to carbon and oxygen, which is one of the crucial processes in FTS. Our DRIFTS results demonstrated that the intensity of the bridge-type CO band located at 1979 cm^{-1} significantly increased with increasing catalyst pore diameter at FTS conditions. With the increase of catalyst pore diameter, the dispersion of cobalt decreased and catalyst reducibility increased, which led to larger cobalt cluster diameter. FTS results show that the activity increased with pore sizes initially then decreased. Consequently, it is suggested that the pore size affected the rate of FTS through affecting the dispersion and catalyst reducibility. It is in accordance with the results of Iglesia et al. [46].

Iglesia et al. [47] have reported that the diffusion limitation has an impact on the performance of FTS if the catalysts particle size is above 0.36 mm. Recently, Holmen and co-workers [13] have found that both the activity and the selectivity were unaffected by the catalyst particle size of less than 225 μm. In the present study, the catalyst particle size is 2–10 μm and no production of gaseous CO_2 has been observed. Thus, effects of diffusion limitation and water–gas shift reaction on C_{5+} selectivity can be excluded. For Co/Re/γ-Al_2O_3 catalysts with different Co particle sizes, a linear relationship between C_{5+} selectivity and particle size has been reported [24]. Because larger cobalt cluster size favors higher C_{5+} selectivity [24,48], wider pore size catalyst exhibited higher C_{5+} selectivity. Besides, C_{5+} selectivity was also found to increase with increasing conversion [24]. Thus, it is reasonable to suggest that the C_{5+} increases with the increase of pore size initially and finally reaches an unchanged value in the range of pore size studied.

4. Conclusions

A series of higher cobalt loading (30 wt.%) on Co/SBA-15 catalysts with different pore sizes, synthesized from the same raw materials, have been prepared and the role of the pore size on FTS has been investigated. After reduction, the cobalt was found to be distributed between both the exterior and interior surfaces of the support. The reduction of the catalysts took place in two stages, with Co_3O_4 reduction to CoO and to Co^0. The reduction of the first stage was facile regardless of the catalyst pore size and much easier reduction of CoO phase to Co was found for the larger pore size catalysts. Compared to small pore size catalyst, wide pore size catalyst exhibited much more CO adsorption sites both linear and bridge type at room temperature. The wider pore size catalysts lead to the formation of larger cobalt cluster size, lower dispersion and higher reducibility. The larger cobalt cluster size gave rise to the enhancement of bridge-type CO during FTS. CO conversion is found to increase and then decrease with increasing pore size studied. The results also show that the cobalt particle size should be of primary importance for the C_{5+} selectivity.

Acknowledgement

This work was supported by National Natural Science foundation of China (20590360, 20773166).

References

[1] A.Y. Khodakov, W. Chu, P. Fongarland, Chem. Rev. 107 (2007) 1692–1744.
[2] E. Iglesia, Appl. Catal. A 161 (1997) 59–78.
[3] P.J. van Berge, J. Van de Loosdrecht, S. Barradas, A.M. van der Kraan, Catal. Today 58 (2000) 321–334.
[4] P.J. van Berge, J. van de Loosdrecht, S. Barradas, A.M. S van der Kraan, Proceedings of the Symp. on Syngas Conversion to Fuels and Chemicals Div. Petr. Chem. 217th Nat'l Meeting of ACS, Anaheim, CA, 1999.
[5] G. Jacobs, Y.Y. Ji, B.H. Davis, D. Cronauer, A.J. Kropf, C.L. Marshall, Appl. Catal. A 333 (2007) 177–191.
[6] D.Y. Zhao, J. Feng, Q. Huo, M. Melosh, G.H. Fredrickson, B.F. Chmelka, G.D. Stucky, Science 279 (1998) 548–552.
[7] A. Martínez, C. López, F. Márquez, I. Díaz, J. Catal. 220 (2003) 486–499.
[8] Y. Wang, M. Noguchi, Y. Takahashi, Y. Ohtsuka, Catal. Today 68 (2001) 3–9.
[9] R.B. Anderson, W.K. Hall, A. Krieg, B. Seligman, J. Am. Chem. Soc. 71 (1949) 183–188.
[10] J.A. Lapszewicz, H.J. Loeh, J.R. Chipperfield, J. Chem. Soc. Chem. Commun. (1993) 913–914.
[11] J. Panpranot, J.G. Goodwin Jr., A. Sayari, J. Catal. 211 (2002) 530–539.
[12] A.Y. Khodakov, A. Griboval-Constant, R. Bechara, V.L. Zholobenko, J. Catal. 206 (2002) 230–241.
[13] Ø. Borg, S. Eri, E.A. Blekkan, S. Storsæter, H. Wigum, E. Rytter, A. Holmen, J. Catal. 248 (2007) 89–100.
[14] G. Jacobs, T. Das, Y.Q. Zhang, J.L. Li, G. Racoillet, B.H. Davis, Appl. Catal. A 233 (2002) 263–281.
[15] H.F. Xiong, Y.H. Zhang, J.L. Li, Y.Y. Gu, J. Cent. S. Univ. Technol. 11 (2004) 414–418.
[16] W.H. Zhang, J.L. Shi, L.Z. Zhang, D.S. Yan, Chem. Mater. 12 (2000) 1408–1413.
[17] A.Y. Khodakov, V.L. Zholobenko, R. Bechara, D. Durand, Microporous Mesoporous Mater. 79 (2005) 29–39.
[18] Centred'Information du Cobalt, in: C.I.C. (Ed.), Cobalt Monograph, C.I.C., Brussel, 1960, p. 170.
[19] A. Moen, D.G. Nicholson, B.S. Clausen, P.L. Hansen, A. Molenbroek, G. Steffensen, Chem. Mater. 9 (1997) 1241–1247.
[20] A. Moen, D.G. Nicholson, M. Ronning, H. Emerich, J. Mater. Chem. 8 (1998) 2533–2539.
[21] J. Bart, Adv. Catal. 34 (1986) 203–297.
[22] D.G. Castner, P.R. Watson, W.L. Dimpfl, SSRL Act. Rep. Proposal No. 628M, 1983, p. VII-57.
[23] G. Jacobs, J.A. Chaney, P.M. Patterson, T.K. Das, B.H. Davis, Appl. Catal. A 264 (2004) 203–212.
[24] S. Storsæter, B. Totdal, J.C. Walmsley, B.S. Tanem, A. Holmen, J. Catal. 236 (2005) 139–152.
[25] P. Li, J. Liu, N. Nag, P.A. Crozier, Appl. Catal. A 307 (2006) 212–221.
[26] M.D. Shannon, C.M. Lok, J.L. Casci, J. Catal. 249 (2007) 41–51.
[27] H.F. Xiong, Y.H. Zhang, S.G. Wang, J.L. Li, Catal. Commun. 6 (2005) 512–516.
[28] N. Tsubaki, S.L. Sun, K. Fujimoto, J. Catal. 199 (2001) 236–246.
[29] F. Morales, E. de Smit, F.M.F. de Groot, T. Visser, B.M. Weckhuysen, J. Catal. 246 (2007) 91–99.
[30] D.C. Song, J.L. Li, Q. Cai, J. Phys. Chem. C 111 (2007) 18970–18979.
[31] L.E.S. Rygh, C.J. Nielsen, J. Catal. 194 (2000) 401–409.
[32] L.E.S. Rygh, O.H. Ellestad, P. Klaeboe, C.J. Nielsen, Phys. Chem. Chem. Phys. 2 (2000) 1835–1846.
[33] D.C. Song, J.L. Li, J. Mol. Catal. A 247 (2006) 206–212.
[34] L. Ji, J. Lin, H.C. Zeng, J. Phys. Chem. B 104 (2000) 1783–1790.

[35] G. Busca, R. Guidetti, V. Lorenzelli, J. Chem. Soc., Faraday Trans. 86 (1990) 989–994.
[36] G. Busca, V. Lorenzelli, R. Guidetti, J. Catal. 131 (1991) 167–177.
[37] A.Y. Khodakov, J. Lynch, D. Bazin, B. Rebours, N. Zanier, B. Moisson, P. Chaumette, J. Catal. 168 (1997) 16–25.
[38] G. Kadinov, C. Bonev, S. Todorova, A. Palazov, J. Chem. Soc., Faraday Trans. 94 (1998) 3027–3031.
[39] M.J. Heal, E.C. Leisegang, R.G. Torington, J. Catal. 51 (1978) 314–325.
[40] A. Lapidus, A. Krylova, V. Kazanskii, V. Borokov, A. Zaitsev, Appl. Catal. 73 (1991) 65–81.
[41] J.L. Li, N.J. Coville, Appl. Catal. A 181 (1999) 201–208.
[42] Z.L. Zhang, A. Kladi, X.E. Verykios, J. Mol. Catal. 89 (1994) 229–246.
[43] S.Y. Chin, C.T. Williams, M.D. Amiridis, J. Phys. Chem. B 110 (2006) 871–882.
[44] H.F. Xiong, Y.H. Zhang, S.G. Wang, K.Y. Liew, J.L. Li, J. Phys. Chem. C 112 (2008) 9706–9709.
[45] E. Iglesia, S.C. Reyes, R.J. Madon, S.L. Soled, Adv. Catal. 39 (1993) 221–302.
[46] E. Iglesia, S.L. Soled, R.A. Fiato, J. Catal. 137 (1992) 212–224.
[47] E. Iglesia, S.L. Soled, J.E. Baumgartner, S.C. Reyes, J. Catal. 153 (1995) 108–122.
[48] G.L. Bezemer, J.H. Bitter, H.P.C.E. Kuipers, H. Oosterbeek, J.E. Holewijn, X. Xu, F. Kapteijn, A.J. van Dillen, K.P. de Jong, J. Am. Chem. Soc. 128 (2006) 3956–3964.